PAPER

Check for updates

The Raman scattering of trirutile structure MgTa$_2$O$_6$ single crystals grown by the optical floating zone method

Dapeng Xu,[a] Shuohui Gao,[c] Wenqiang Liu,[ad] Ying Liu, [ID][a] Qiang Zhou,[a] Liang Li, [ID] *[ab] Tian Cui [ID][a] and Hongming Yuan [ID][e]

Single crystals of the trirutile structure MgTa$_2$O$_6$ were grown *via* an optical floating zone method in an air atmosphere. The as-grown crystals were pale yellow and transparent and the natural cleavage plane formed during the crystal growth was determined by XRD2 to be along the *c*-axis direction. The variations in valence were investigated by XPS (X-ray photoelectron spectroscopy). The room-temperature axis-relative polarized Raman spectra of trirutile MgTa$_2$O$_6$ crystals were described. The order−disorder effect was detected *via* temperature-dependent Raman spectroscopy.

Introduction

MgTa$_2$O$_6$ is a typical dielectric oxide that exhibits excellent microwave dielectric properties and has attracted significant attention for its application in microwave resonators, filters, microstrip antennas and waveguides in the past decade.[1,2] It has a general formula of AB$_2$O$_6$, which has been reported to crystallize in the trirutile structure with space group of *P*4$_2$/*mnm* and tetragonal lattice parameters of $a = b = 4.7189(7)$ Å and $c = 9.2003(22)$ Å. The crystal structure is described by a unit cell that is triple the conventional rutile unit cell along the tetragonal *c*-axis. The cations, which occupy half of the octahedral available sites, are surrounded by O^{2-} organized in a hexagonal close-packed arrangement. This yields a chemically ordered network of interpenetrating edge and corner-sharing slightly distorted octahedrons. More recently, studies have focused attention on MgTa$_2$O$_6$ for use as a UV-light active material for water splitting by narrowing the band gap through nitrogen doping.[3,4] Moreover, the trirutile structure of MgTa$_2$O$_6$ has been achieved in optically uniaxial crystals with large birefringence, and has been increasingly used as polarizers in optical communications and other optical devices.[5,6]

Furthermore, Raman scattering involves the inelastic scattering of light. The frequency of a photon can change by transferring energy to and/or receiving energy from the lattice vibrations of the materials. In quantum mechanics, the "allowed" energies of oscillation are quantized and are equidistant in the case of a harmonic oscillation. The vibrations of the lattice can thus be described as quasi-particles and the term phonon is usually used; thus, Raman scattering is sensitive to the crystal lattice vibrations. The Raman spectra are usually used to study the structures of solids *via* their vibrational properties.[7,8] Examination of the line shapes in Raman spectra may yield useful information concerning the crystallinity and amorphicity of the materials and therefore, Raman spectra are of great value for the further understanding of materials.

Single crystals with well-defined crystallographic orientations and appropriate sizes are suitable for many diverse applications in solid-state and quantum electronics as well as for the detailed study of the intrinsic physical properties of materials.[9–12] Higuchi *et al.* reported the crystal growth of MgTa$_2$O$_6$ by the floating zone method under an argon atmosphere and gave some optical properties; however, the as-grown crystals were black due to oxygen vacancies, which can affect the quality of the crystals.

In the current work, MgTa$_2$O$_6$ single crystals with the trirutile structure have been grown by the optical floating zone method in air, and pale yellow MgTa$_2$O$_6$ single crystals were directly achieved. X-ray photoelectron spectroscopy (XPS) was performed on both as-grown and argon atmosphere-annealed samples to verify the effect of the oxygen vacancies in the crystals. By adopting the proper polarization direction of the incident and scattered light, an oriented single crystal could activate specific vibration modes. Therefore, the polarized Raman spectra of single crystals can precisely identify the vibrational mode, which cannot be identified from non-polarized Raman spectra with similar wavenumbers. In spite of this, only nonpolarized Raman spectra of MgTa$_2$O$_6$ powder samples were reported by Husson *et al.*[13,14] The optical phonon behaviors of the obtained MgTa$_2$O$_6$ crystals were also studied

[a] State Key Laboratory of Superhard Materials, College of Physics, Jilin University, Changchun, Jilin, China. E-mail: lliang@jlu.edu.cn

[b] College of Mechanical Engineering, University of Texas at Austin, Austin, Texas, USA

[c] China-Japan Union Hospital of Jilin University, Changchun, 130000, P. R. China

[d] College of Physics, Harbin Institute of Technology, Harbin, Heilongjiang, China

[e] State Key Laboratory of Inorganic Synthesis and Preparative Chemistry, College of Chemistry, Jilin University, Changchun, Jilin, China

through Raman spectra at different polarized configurations. Herein, aiming to explore opportunities for applying $MgTa_2O_6$ materials at different temperatures, the in-site temperature-dependent Raman spectra of $MgTa_2O_6$ crystals are investigated for the first time.

Experimental

The fabrication of $MgTa_2O_6$ supporting and feeding rods began with the calcination of ground powders containing stoichiometric amounts of MgO (Alfa Aesar 99.99%) and Ta_2O_5 (Alfa Aesar 99.99%) at 1400 K for 20 h with intermediate grinding. The obtained $MgTa_2O_6$ powder was then packed into cylindrically shaped rubber tubes, evacuated *via* a vacuum pump, and then hydrostatically pressed, up to 75 MPa, in a cold isostatic presser to form a cylindrical rod of 0.6–0.8 cm in diameter and about 10 cm in length. The rods were sintered in air at 1700 K for 10 h.

The crystal growth was conducted in an optical floating zone furnace with four 1000 W halogen lamps as heating sources (CSI FZ-T-10000-H-VI-VP, Crystal systems, Inc., Japan). The growth conditions are as follows: the growth speed was 6 mm h^{-1}; the support and feed rods were rotated 10 rpm in opposite directions; the air flow was about 0.5 L min^{-1} with a pressure of 0.2 MPa.

The structure of the samples was characterized using a Rigaku RU-200b X-ray diffractometer (XRD) with Cu Kα radiation. A Rigaku Micro Max-007HF X-ray diffractometer (XRD2) was used to probe the orientation of the as-grown crystals. The X-ray photoelectron spectra (XPS) were taken on an ESCALAB 250 electron energy spectrometer with Mg Kα (12 530.6 eV) as the X-ray excitation source. The Raman spectra of the samples were obtained by using a Jobin-Yvon LABRAM-HR 800 spectrometer equipped with a Peltier-cooled CCD detector with a confocal 50× objective Olympus microscope. The spectral resolution and the lateral resolution used were approximately 1 cm^{-1} and 2 μm, respectively. All the Raman measurements were conducted in a backscattering geometry configuration by using the 514.5 nm line from an adjustable Ar ion laser with 20 mW power (Spectra-Physics Stabilite 2017) as the excitation source. An edge filter for the stray light rejection was also used. The temperature-dependent Raman spectra were achieved by using the THMSE 600 cooling & heating stage (Linkam Scientific Instruments) attached to the Raman spectrometer in the temperature range from 89 to 778 K.

Results and discussion

Based on our previous experience with the growth of this series of crystals,[15,16] the $MgTa_2O_6$ crystals were grown in an air atmosphere. After the optimization of the growth parameters, including the growth speed, rotation speed and lamp power, the $MgTa_2O_6$ crystals were successfully grown with several large domains. The as-grown $MgTa_2O_6$ crystals were light yellow in color. The largest crystal domain was 6 × 3 × 10 mm in size, which included a natural cleavage plane formed during the crystal growth as shown in the inset of Fig. 1b. The as-grown
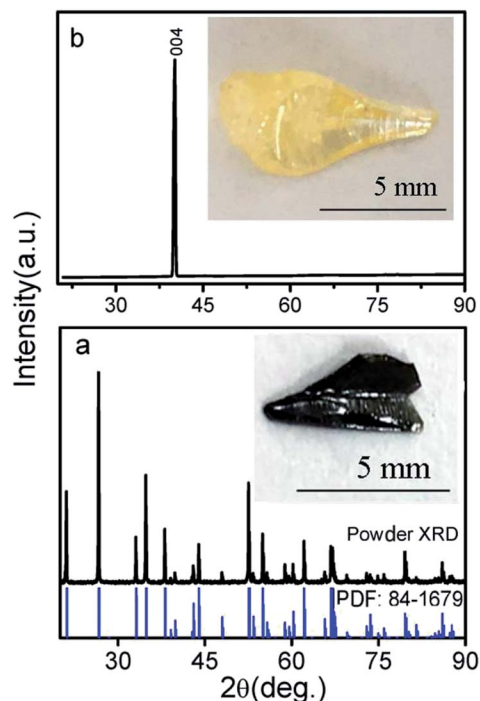

Fig. 1 (a) Powder XRD of crushed $MgTa_2O_6$ single crystals; the inset shows the argon-annealed crystal. (b) XRD2 of the natural cleavage plane parallel to the growth direction; the inset shows the as-grown crystal.

$MgTa_2O_6$ crystals were then crushed to a powder to obtain detailed structural information. The powder X-ray diffraction (XRD) pattern shown in Fig. 1a indicates that all peaks can be indexed to the diffraction peaks of trirutile $MgTa_2O_6$ (PDF no.: 84-1679, as shown in the bottom of Fig. 1a). The natural cleavage plane parallel to the growth direction was tested by XRD2 as shown in Fig. 1b, in which only one peak, located at 39.1° and indexed as the ⟨004⟩ plane, was observed. These results indicate that a single phase of $MgTa_2O_6$ can be confirmed and the crystal cleavage was along the *c*-axis direction.

The as-grown $MgTa_2O_6$ crystals were annealed in an argon atmosphere at 1773 K for 10 hours. The annealed samples were black and transparent, as shown in the inset of Fig. 1a. In order to gain more insight into the physical mechanism and the effects of the argon atmosphere on the samples, XPS was performed on the as-grown and annealed samples. Fig. 2 shows the Ta 4f peaks from the XPS results. An obvious shift of the two Ta 4f half peaks 4f$_{5/2}$ and 4f$_{7/2}$ to higher energy levels was observed, indicating the valence reduction of the Ta element.

The trirutile structure $MgTa_2O_6$ belongs to the tetragonal lattice with the space group: $P4_2/mnm$ (no. 136) or point group D_{4h} (4/mmm). A total of 18 atoms exist in the primitive cell, which corresponds to 54 degrees of freedom. The irreducible representations of the D_{4h} (4/mmm) point group at the Γ-point of the first Brillouin zone can be obtained as follows:[14]

$$\Gamma = 4A_{1g} + 2A_{2g} + 2B_{1g} + 4B_{2g} + 6E_g + A_{1u} + 4A_{2u} + 5B_{1u} + B_{2u} + 8E_u,$$
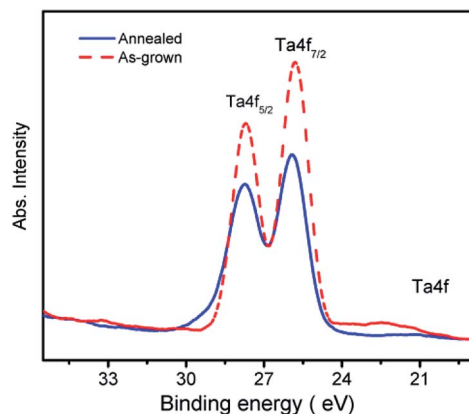
Fig. 2 The XPS spectra of Ta 4f peaks of the as-grown and argon-annealed crystals.
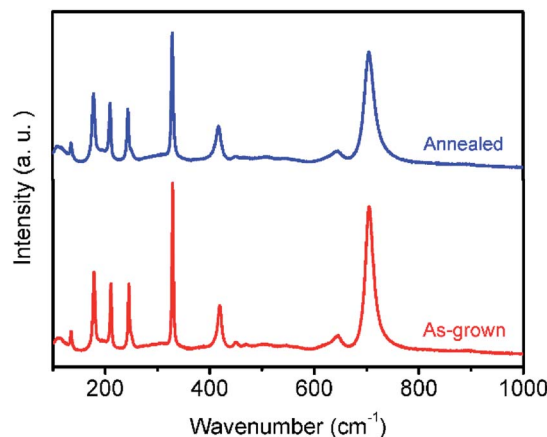

Fig. 3 Room temperature Raman spectra of crushed as-grown and annealed $MgTa_2O_6$ samples.

in which the Raman-active modes are $\Gamma_{Raman} = 4A_{1g} + 2B_{1g} + 4B_{2g} + 6E_g$ with the following Raman tensors:[17]

$$A_{1g} = \begin{pmatrix} a & 0 & 0 \\ 0 & a & 0 \\ 0 & 0 & c \end{pmatrix}; B_{1g} = \begin{pmatrix} c & 0 & 0 \\ 0 & -c & 0 \\ 0 & 0 & 0 \end{pmatrix};$$

$$B_{2g} = \begin{pmatrix} 0 & d & 0 \\ d & 0 & 0 \\ 0 & 0 & 0 \end{pmatrix}; E_g = \begin{pmatrix} 0 & 0 & 0 \\ 0 & 0 & e \\ 0 & e & 0 \end{pmatrix}; E_g = \begin{pmatrix} 0 & 0 & -e \\ 0 & 0 & 0 \\ -e & 0 & 0 \end{pmatrix}$$

The Raman tensors are significant in the polarized Raman investigation of materials, especially in spectrum-scattering intensity, which is directionally dependent upon an intrinsic coordinate system.[8,18] In this study, the a, b, and c-axes of the crystal lattices are expressed as X, Y, and Z. To analyze a component α_{ij} of a given tensor, the incident light should be configured to polarized along the i direction and the scattering light can only be observed when polarized along the j direction. Hence, according to Raman tensor and polarization selection rules, in the XX, YY, and ZZ polarized configurations, the incident scattering lights are parallel with the direction of a specific crystalline axis, and A_{1g} modes can be detected. B_{1g}, B_{2g}, and E_g correspond to XX and YY; XY and YX; YZ and ZY, XZ and ZX, respectively.

To further investigate the oxygen vacancy effect on the properties of the sample, the as-grown and the argon annealed $MgTa_2O_6$ were crushed to powder. Powder Raman spectra were obtained under the same conditions for both the crushed as-grown and argon annealed $MgTa_2O_6$ powder samples, as shown in Fig. 3. The spectra presented typical bands corresponding to the normal vibration modes of $MgTa_2O_6$.[14] The maximum phonon model at 704 cm^{-1} can be indexed to the Ta–O stretching band. The position of the model was 704.3 for the annealed sample and 704.9 for the as-grown sample. The linewidths (FWHM) for the peak at 704 cm^{-1} of the as-grown and annealed sample were fitted to be 18 and 22 cm^{-1}, respectively. The 704 cm^{-1} spectrum broadening and lower energy of the argon annealed sample can be attributed to the partial reduction of Ta^{5+} ions caused by the oxygen vacancies, resulting in the

change in the Ta–O stretching vibration. This result agrees well with the XPS data.

The parallel-polarized (XX, YY, and ZZ configuration) and cross-polarized (XY, YZ, and XZ configuration) Raman spectra of $MgTa_2O_6$ were achieved as shown in Fig. 4 and 5, respectively. All Raman peaks in the spectra can be indexed in the range from 150 to 1000 cm^{-1}, except for the peak at 210 cm^{-1}, which has not been indexed in previous work. No B_{1g} and B_{2g} mode was observed in the figures; for all figures, blue and red font represent the E_g and A_{1g} modes, respectively. In the XX, YY, and ZZ polarization, the strongest peaks were located at 704 cm^{-1}, which can be indexed to the TaO_6 octahedron-symmetrical stretching vibration peaks of the A_{1g} mode. In the YZ, and XZ configuration, the spectra are dominated by the peak located at 329 cm^{-1}, which can be indexed as the E_g mode. Notably, there are only three indexed Raman peaks in the XY polarization, dominated by 210 cm^{-1}, which is an unindexed mode. No indexed B_{2g} mode, the expected mode in the XY configuration,

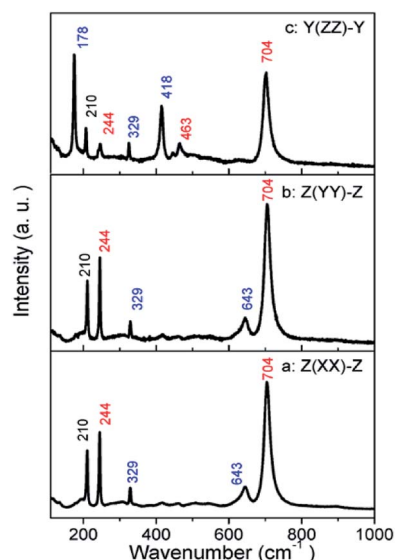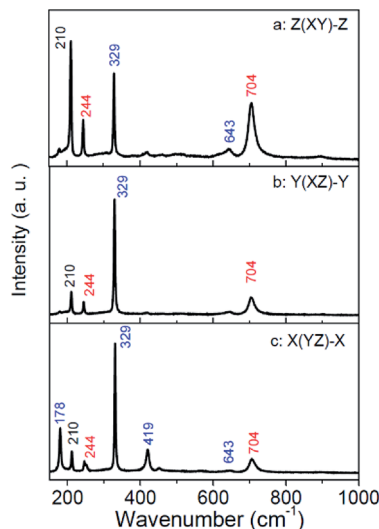**Fig. 4** Parallel-polarized Raman spectra for the $MgTa_2O_6$ crystal: (a) Z(XX)-Z; (b) Z(YY)-Z; (c) Y(ZZ)-Y.

Fig. 5 Cross-polarized Raman spectra for the MgTa$_2$O$_6$ crystal: (a) Z(XY)-Z; (b) Y(XZ)-Y; (c) X(YZ)-X.

was detected. Thus, a conclusion can be drawn that the mode at 210 cm^{-1} should be indexed to the B$_{2g}$ mode.

The peaks appear in the polarized configuration, to which they do not belong, and the different relative intensities of the same modes under different parallel-polarized configuration can be explained in terms of the structure of the sample. The structure of trirutile MgTa$_2$O$_6$ is very complicated. Given the orientations and distortions of the oxygen octahedron and the parallel link with the b-axis between MgO$_6$ and TaO$_6$ octahedron, the internal field is anisotropic. The dazzling effect of the lens is another influencing factor; the strong leakage of the E$_g$ modes can be attributed to this.[19]

In-site temperature-dependent Raman spectra were measured on a small crystallite sample size of 1 μm^3, taken from the crushed MgTa$_2$O$_6$ crystals, to obtain a rapid thermal response. A total of 24 temperature-measurement points were observed every 30 K from 89 to 778 K. Raman spectra obtained at selected temperatures are shown in Fig. 6. At 89 K, a total of
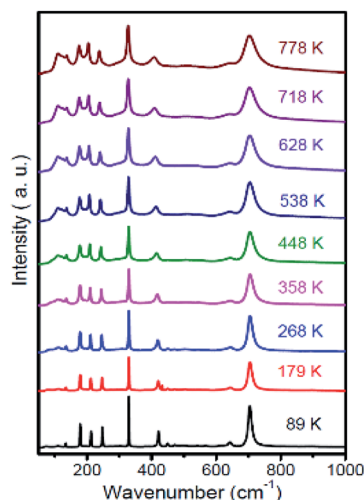
11 identifiable Raman peaks were observed. An increase in temperature caused the Raman peaks to move to lower wavenumbers with continuous linewidth broadening and a decrease in intensity. Notably, during the procedure, a new bond located at 110 cm^{-1} appeared when the temperature increased to 358 K, and the new bond became stronger and shifted toward lower wavenumbers with increasing temperature. The relative intensity of the bond located at 210 cm^{-1} was lower as compared to the nearest two bonds located at 178 and 244 cm^{-1} when the temperature was lower than 358 K. Accompanied by the appearance of the new bond, the bond located at 210 cm^{-1} become stronger than the nearest two bonds. With the increasing temperature, the atoms may move to other sites under the thermal effect. The Ta^{5+} and Mg^{2+} ions, in the TaO$_6$ and MgO$_6$ octahedrons, exchanged slightly. The lower bond located at 110 cm^{-1} could be attributed to extra bond Ta–Mg vibration replacing the non-Raman active Ta–Ta bond. Higher Raman active Ta–O substituted for lower Raman active Mg–O bonds, resulting in the bond at 210 cm^{-1} becoming stronger. This can be attributed to the order–disorder effect.

Conclusions

MgTa$_2$O$_6$ single crystals having the trirutile structure were grown via the optical floating zone method. The as-grown crystals were light yellow and transparent. The largest crystal domain was 6 × 3 × 10 mm with a natural cleavage plane formed during the crystal growth, tested as the c-axis direction. XPS and powder Raman spectra results indicated the increase in the oxygen vacancy after annealing in the argon atmosphere. The corresponding polarized Raman spectra of MgTa$_2$O$_6$ crystals were obtained using adequate parallel and crossed configurations. All the obtained Raman modes were identified and were in good agreement with previous normal coordinate analysis. The selection rules for the trirutile group were validated. The temperature-dependent Raman spectra show an order–disorder effect in the temperature range.

Conflicts of interest

There are no conflicts to declare.

Acknowledgements

Notes and references

1 D. Grosso, C. Boissiere, B. Smarsly, T. Brezesinski, N. Pinna, P. A. Albouy, H. Amenitsch, M. Antonietti and C. Sanchez, Nat. Mater., 2004, 3, 787–792.

Fig. 6 Temperature-dependent Raman spectra of MgTa$_2$O$_6$ crystals.

2 S. S. Chen, Y. Qi, G. J. Liu, J. X. Yang, F. X. Zhang and C. Li, *Chem. Commun.*, 2014, **50**, 14415–14417.

3 T. F. Liu, M. Dupuis and C. Li, *J. Phys. Chem. C*, 2016, **120**, 6930–6937.

4 S. Chen, Y. Qi, T. Hisatomi, Q. Ding, T. Asai, Z. Li, S. S. K. Ma, F. Zhang, K. Domen and C. Li, *Angew. Chem.*, 2015, **127**, 8618–8621.

5 H. Mikio, A. Kazuto, T. Junichi and K. Kodaira, *J. Ceram. Soc. Jpn.*, 1993, **101**, 118–120.

6 O. I. Velikokhatnyi, K. Kadakia, S.-K. Park and P. N. Kumta, *J. Electrochem. Soc.*, 2012, **159**, F607–F616.

7 F. Herziger, M. Calandra, P. Gava, P. May, M. Lazzeri, F. Mauri and J. Maultzsch, *Phys. Rev. Lett.*, 2014, **113**, 187401.

8 N. V. Vitanov, A. A. Rangelov, B. W. Shore and K. Bergmann, *Rev. Mod. Phys.*, 2017, **89**, 015006.

9 L. Li, D. Duan, Q. Zhou, D. Xu, T. Cui, B. Liu, Z. Shi and H. Yuan, *J. Alloys Compd.*, 2015, **619**, 240–243.

10 W. A. Phelan, S. M. Koohpayeh, P. Cottingham, J. A. Tutmaher, J. C. Leiner, M. D. Lumsden, C. M. Lavelle, X. P. Wang, C. Hoffmann, M. A. Siegler, N. Haldolaarachchige, D. P. Young and T. M. McQueen, *Sci. Rep.*, 2016, **6**, 10.

11 K. E. Arpino, B. A. Trump, A. O. Scheie, T. M. McQueen and S. M. Koohpayeh, *Phys. Rev. B*, 2017, **95**, 8.

12 R. Loudon, *Adv. Phys.*, 1964, **13**, 423–482.

13 E. Husson, Y. Repelin, H. Brusset and A. Cerez, *Spectrochim. Acta, Part A*, 1979, **35**, 1177–1187.

14 E. Husson, Y. Repelin and H. Brusset, *J. Solid State Chem.*, 1980, **33**, 375–384.

15 L. Li, G. Feng, D. Wang, H. Yang, Z. Gao, B. Li, D. Xu, Z. Ding and X. Liu, *J. Alloys Compd.*, 2011, **509**, L263–L266.

16 L. Li, W. Liu, B. Han, X. Jin, F. Li, W. Wang, Q. Zhou, D. Xu and T. Cui, *RSC Adv.*, 2015, **5**, 66988–66993.

17 E. Kroumova, M. I. Aroyo, J. M. Perez-Mato, A. Kirov, C. Capillas, S. Ivantchev and H. Wondratschek, *Phase Transitions*, 2003, **76**, 155–170.

18 D. Xu, W. Liu, Q. Zhou, T. Cui, H. Yuan, W. Wang, Y. Liu, Z. Shi and L. Li, *J. Appl. Phys.*, 2014, **116**, 083509.

19 N. G. Teixeira, R. L. Moreira, M. R. B. Andreeta, A. C. Hernandes and A. Dias, *Cryst. Growth Des.*, 2011, **11**, 3472–3478.